

INVESTIGATION ON THE MECHANICAL BEHAVIOUR OF HYBRID FIBRE REINFORCED POLYMER COMPOSITE BEAM

G.B. Maranan and A.C. Manalo

Centre of Excellence in Engineered Fibre Composites,
University of Southern Queensland, Toowoomba, Queensland, Australia
Email: Ging.Maranan@usq.edu.au, allan.manalo@usq.edu.au

ABSTRACT

Fibre reinforced polymer (FRP) composites have been proven a viable alternative to conventional construction materials such as timber, steel, and reinforced concrete due to its high strength-to-weight, light weight, durable, and corrosion resistant properties. Several studies suggested the effective use of FRP composites in sandwich structures. This paper presents the physical and mechanical properties of a sandwich-structured glue-laminated beam, named as hybrid FRP composite beam, developed by CarbonLOC Pty Ltd in cooperation with the Centre of Excellence in Engineered Fibre Composites (CEEFC) in University of Southern Queensland (USQ). This beam combines the strength and stiffness of glue-laminated panels oriented in the edgewise position bonded with the high tensile strength and modulus Glass Fibre Reinforced Polymer (GFRP) skin plates at the top and bottom. The average experimental failure loads of the beam in flexure, shear, longitudinal compression, and tangential compression are 53.45 kN, 211.73 kN, 450.06 kN, and 220.31 kN, respectively, which corresponds to strength of 106.90 MPa, 35.29 MPa, 75.01 MPa, and 61.20 MPa, respectively. The effective stiffness of the beam was enhanced due to top and bottom GFRP plates. Theoretical prediction showed reasonably comparable failure load with the experimental results.

KEYWORDS

FRP composites, sandwich structures, hybrid beam, shear, flexure, compression.

INTRODUCTION

Fibre reinforced polymer (FRP) composites have been proven a viable alternative to most commonly used construction materials such as timber, steel, and reinforced concrete. Ideal properties of this material include high strength-to-weight, light weight, durable and corrosion resistant (Barbero 1999) which can be incorporated in the production of different structural elements, like beams or girders, for civil infrastructure applications. Several studies have proven the usability of FRP composites in sandwich structures (e.g. Flores-Johnson *et al.* 2012; Zhou *et al.* 1999; Kim *et al.* 1999). Further, glue-laminating in sandwich structure was adapted from the design of glue-laminated (glulam) timber beams wherein a single large and strong structural member is made by laminating together smaller pieces of timber. The strongest laminations are placed at the top and bottom since the maximum tensile and compression stresses occurred in these locations (APA EWS 1996).

In Australia, the Centre of Excellence in Engineered Fibre Composites (CEEFC) in the University of Southern Queensland (USQ) in collaboration with various industries and state governments have been involved in the research and project development on FRP composites. An example of these projects is the development of novel FRP composite sandwich panels made up of glue-laminated modified phenolic core with two thin but stiff GFRP skin plates. Manalo *et al.* (2009, 2010) examined the physical and mechanical properties of these panels oriented in edgewise and flatwise directions including the behaviour of these sandwich panels when glued together. While the experimental results showed comparable strength properties of the composite sandwich panels with structural timber, the glued sandwich panels has an effective stiffness of only 4GPa, which is suitable for railway turnout sleeper application. However, a higher stiffness is required in structural beam application where the design using FRP materials is governed mostly by serviceability requirement rather than strength.

Recently, CarbonLOC Pty. Ltd in cooperation again with CEEFC, had fabricated a sandwich-structured beam with new configuration and is made up of component materials used in their previous projects. This hybrid FRP composite beam combines the strength and stiffness of edgewise-oriented sandwich panels glued together using

toughened phenol formaldehyde resin, with high tensile strength and modulus top and bottom GFRP skin plates (see Figure 1). In this concept, the glued sandwich beams in the edgewise position is anticipated to provide the required shear strength while the top and bottom GFRP plates provide the needed stiffness. This paper presents the physical and mechanical properties of this beam through three-point static bending test, asymmetrical beam shear test, longitudinal compressive test, and tangential compressive test.

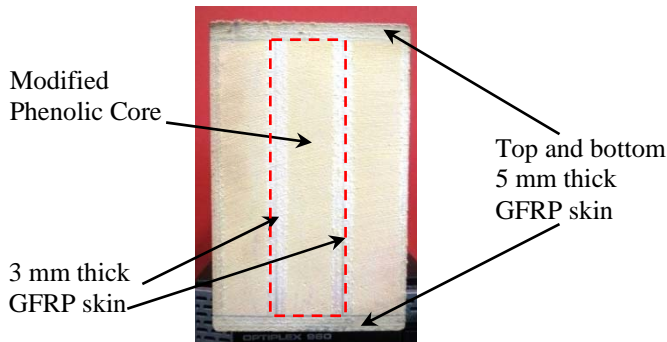


Figure 1. Hybrid FRP composite beam

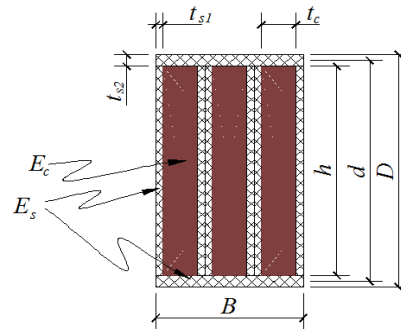


Figure 2. Schematic diagram of hybrid FRP composite beam

EXPERIMENTAL PROGRAM

Properties and dimensions of component materials

Characterization of the integral materials of the hybrid composite beam such as 3 mm and 5 mm thick biaxial ($0^\circ/90^\circ$) GFRP plates and modified phenolic core was done by Manalo (2011) and is summarized in Table 1. The nominal width (B) and total height (D) of the beam are 60 mm and 100 mm, respectively. The specimens were provided by the industry partner and cut according to required dimensions for each each test. Figure 2 shows the schematic diagram of the beam with its dimensions. Three specimens were prepared for each test and were labeled as HB-F, HB-S, HB-LC, and HB-TC. HB stands for hybrid beams while F, S, LC and TC correspond to three-point static bending test, asymmetrical beam shear test, longitudinal compression test, and transverse compression test, respectively. Tables 2 and 3 summarized the dimensions of specimens and its constituent materials, respectively.

Table 1. Characteristics of GFRP skin and phenolic core

Test	Property	GFRP skin		Phenolic Core
		Longitudinal direction	Transverse Direction	
Flexure	Modulus (GPa)	(E_s) 12.82	3.66	(E_c) 1.33
	Peak stress (MPa)	317.37	135.05	14.32
Tensile	Modulus (GPa)	15.38	12.63	1.03
	Peak stress (MPa)	247.24	216.27	5.97
Compression	Modulus (GPa)	16.10	9.95	1.33
	Peak stress (MPa)	(σ_{ics}) 201.75	(σ_{ics}) 124.23	21.35
Shear	Modulus (GPa)	2.47	2.17	0.52
	Peak stress (MPa)	23.19	(τ_{ts}) 21.81	4.54

Note: The values with indicated parameters are used in failure load estimation

Table 2. Dimensions and label of specimens

Label	Length, L (mm)	Width, B (mm)	Height, D (mm)
HB-F	1000	60	100
HB-S	400	60	100
HB-LC	120	60	100
HB-TC	60	60	100

Table 3 Dimensions of constituent materials

Parameter	Dimension (mm)
Core thickness, t_c	14
Skin thickness, t_{s1}	3
Skin thickness, t_{s2}	5
Beam width, B	60
Height of sandwich panel, h	90
$d = h + t_{s2}$	95
$D = h + 2 t_{s2}$	100

Test set-up and procedures

The three-point static bending test was performed following ASTM C393-00 (refer to Figure 3). The simply supported specimens, with clear span (L_f) of 800 mm (equivalent to 8 times its depth), are loaded at midspan at a

rate of 2 mm/min using SANS hydraulic testing machine. On the other hand, the shear strength of beam was determined based on asymmetrical beam shear test. The set-up shown in Figure 4 is a modification of Iopescu shear test for composites. The specimens are loaded at a rate of 1 mm/min using the same machine. For both tests, steel plates were placed at points of load application and at supports to prevent local indentation failure. ASTM C364 was adapted to determine the longitudinal and transverse compression properties of the beam (see Figures 5 and 6). Utilizing the same machine, the load is applied at a rate of 1 mm/min. The applied load and displacement in all tests were recorded using the built-in data logger of the machine.

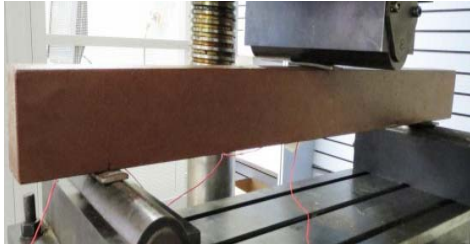


Figure 3. Three-point static bending test

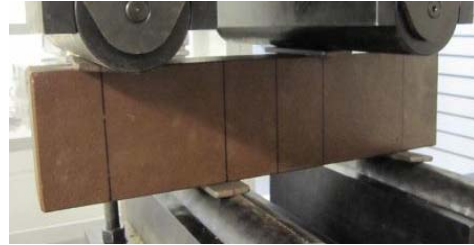


Figure 4. Asymmetrical beam shear test



Figure 5. Longitudinal compression test



Figure 6. Transverse compression test

RESULTS AND DISCUSSION

Flexural Behaviour

The load and midspan deflection relationship of the specimens in three-point static bending test are shown in Figure 7. From the figure, the applied load increases linearly with deflection at an early stage. As the load is further increased, cracks began to form at the top of the beams that resulted into marginal drops in their load-carrying capacities and stiffness. The maximum load and deflection sustained by HB-F-1 are 46.01 kN and 20.48 mm, respectively. On the other hand, HB-F-2 carried a maximum load of 55.84 kN and a deflection of 23.07 mm while HB-F-3 reached a maximum load of 58.49 kN with deflection of 28.94 mm. The average flexural load is 53.45 kN which corresponds to flexural strength of 106.90 MPa. Further, the computed effective stiffness of the hybrid beam is 5.61 GPa. This 1.61 GPa increase in the effective stiffness of the beam is attributed to the additional stiffness provided by top and bottom GFRP plates to glued sandwich panels. The typical external failure of beams in flexure is shown in Figure 8a. Right after reaching the peak load, delamination and buckling of top GFRP skin and vertical cracks in external skin of the sandwich panels occurred. The beam continued to carry additional loads due to its bottom GFRP skin that leads into fibre pullout at the bottom of the beam. However, the phenolic core remained intact after failure (see Figure 8b) which suggests that flexural failure of beam is governed by compression failure of top GFRP skin.

Shear Behaviour

Figure 9 shows the load and deflection relationship of specimens in asymmetrical beam shear test. As depicted in the graphs, linear elastic behaviour is exhibited by all specimens at lower loads. At higher loads, nonlinearity and stiffness degradation are observed due to local indentation in the beam at the points of loading and supports. HB-S-3 recorded the highest value of shear load roughly equivalent to 220.38 kN. The peak loads of HB-S-1 and HB-S-2 are 211.32 kN and 203.49 kN, respectively. The mean shear load and strength capacity of the beam are 211.73 kN and 35.29 MPa. Figure 10a shows the typical external shear failure of the specimens. Generally, shear stresses are resisted by the tensile strength of top and bottom GFRP skins and shear strength of external skins as evidenced by delamination of top and bottom GFRP skins and vertical cracks in outermost skins of sandwich panels. Once these strengths are exceeded, the remaining shear loads are carried by phenolic cores that lead into their severe cracking as shown in Figure 10b.

Longitudinal Compression Behaviour

The longitudinal compressive load and deformation diagrams of the specimens are shown in Figure 11. At early stage, linear elastic behaviour is observed in the specimens. The maximum compressive loads sustained by HB-LC-1, HB-LC-2 and HB-LC-3 are approximately 484.81 kN, 462.21 kN and 403.12 kN (average of 450.05 kN) with deflections of 3.96 mm, 4.20 mm and 4.40 mm, respectively. The average longitudinal compressive strength of the beam is computed as 75.01 MPa. At failure, pronounced delamination and buckling are exhibited by the top and bottom GFRP skins (see Figure 12). Cracks are also formed in the outermost skin of sandwich panels. However, the core and internal GFRP skins remained intact. These observations suggest the idea that the longitudinal compression failure of the beam is governed by the failure of top and bottom GFRP skin. In addition, brittle mode of failure is observed in all specimens.

Transverse Compression Behaviour

Figure 13 show the graphs of the transverse compressive load and deformation of the specimens. The load is directly proportional to the deflection at lower loads. Reduction of stiffness and nonlinearity behaviour occurred before reaching the peak loads. These are due to delamination of the external skins of sandwich panel. The maximum sustained loads and corresponding deformations of HB-TC-1, HB-TC-2, and HB-TC-3 are 220.04 kN and 2.90 mm, 224.33 kN and 2.89 mm, and 216.55 kN and 3.08 mm, respectively. The average peak load recorded is 220.31 kN. This corresponds to average transverse compression strength of 61.20 MPa. The failures of specimens in this test are governed by delamination of external GFRP skins followed by formation of diagonal shear cracks in the phenolic core (refer to Figure 14).

Estimation of Failure Load

The failure loads of specimens in each test were estimated adapting the following assumptions: 1) fibre composite skins and core material are assumed to behave linearly elastic up to failure; 2) perfect bonding exists among the component materials; and 3) delamination in constituent materials does not occur. Equations 1 to 4 were used to estimate the failure load of the hybrid composite beam. The flexural failure load of beam was estimated using equation 1 that was derived based on Euler-Bernoulli equation for simply supported beam. The predicted bending load (P_f) of the beam is 54.74 kN. On the other hand, equation 2 was used to predict the shear load failure (P_s) of the beam. The estimated shear load is 121.20 kN. The longitudinal compression failure of the beam was estimated using equation 3. The theoretical failure load (P_{lc}) is 527.00 kN. Finally, the failure load in tangential compression is computed using equation 4 and is equivalent to 166.67 kN. The dimension m represents the length of specimen (60 mm).

$$P_f = \frac{8\sigma_{lcs} \left[\left(\frac{t_{s1}h^3}{2} E_s + \frac{t_c h^3}{4} E_c \right) + \left(\frac{Bt_{s2}^3}{6} + \frac{Bt_{s2}d^2}{2} \right) E_s \right]}{L_f D E_s} \quad (1)$$

$$P_s = 2\tau_{ts} \left[3 \left(2t_{s1} + t_c \frac{E_c}{E_s} \right) h + 2Bt_{s2} \right] \quad (2)$$

$$P_{lc} = \sigma_{lcs} \left[3 \left(2t_{s1} + t_c \frac{E_c}{E_s} \right) h + 2Bt_{s2} \right] \quad (3)$$

$$P_{tc} = \sigma_{tcs} \left[3 \left(2t_{s1} + t_c \frac{E_c}{E_s} \right) m \right] \quad (4)$$

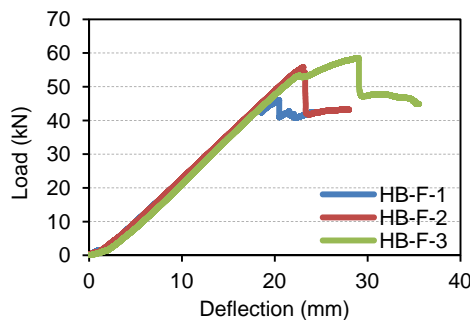


Figure 7. Load-deflection diagram of the beam under three-point bending test

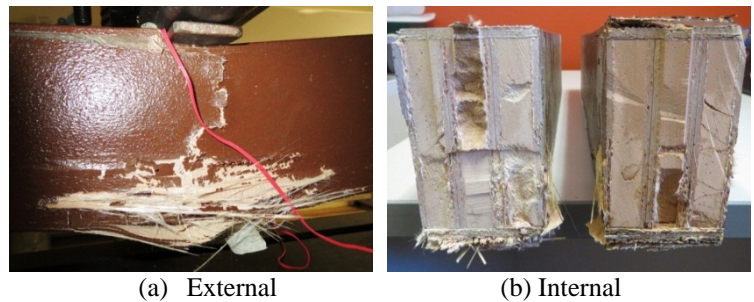


Figure 8. External and internal flexural failure of hybrid FRP composite beam

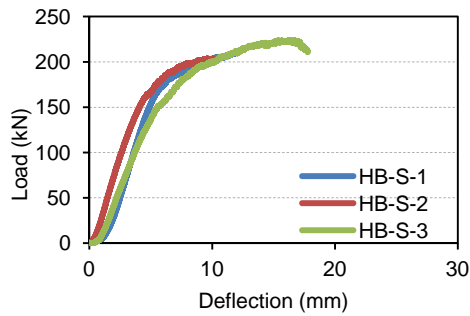
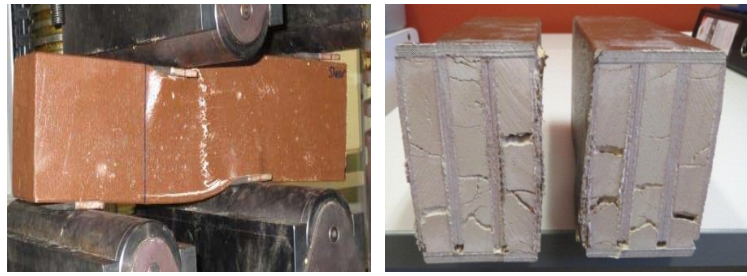


Figure 9. Load-deflection diagram of the beam under asymmetrical beam shear test



(a) External (b) Internal
Figure 10. External and internal shear failure of hybrid FRP composite beam

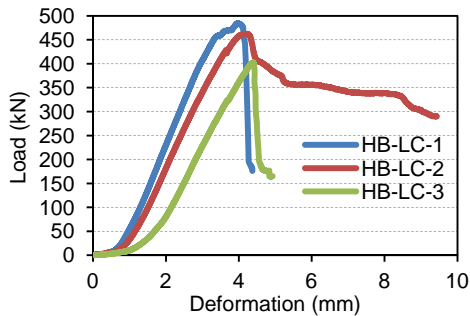


Figure 11. Longitudinal compressive load-deformation diagram of hybrid FRP beam



Figure 12. Failure in longitudinal compression of hybrid FRP composite beam

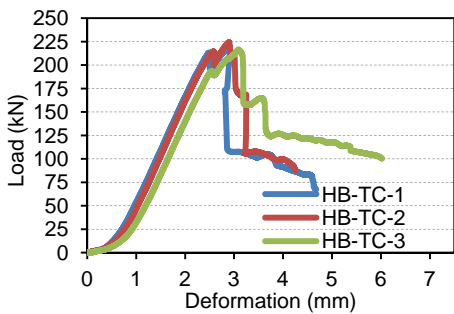


Figure 13. Transverse compressive load-deformation diagram of hybrid FRP beam



Figure 14. Failure in transverse compression of hybrid FRP composite beam

Comparison and Evaluation of Failure Loads

Table 4 summarizes the experimental and theoretical failure load of specimens in each test. The estimated maximum failure loads in flexure and longitudinal compression are marginally higher than experimental values because GFRP skins delaminated before reaching the estimated loads. On the other hand, experimental shear load failure is higher than theoretical prediction because even though the transverse shear strength of 5 mm top and bottom GFRP skins are exceeded, the skins continued to resist stresses through its tensile strength (as evidenced by buckling and delamination failure in the GFRP skins). The tensile strength of these skins together with shear strength of vertically-oriented skins of sandwich panels had resulted into higher experimental shear load failure as compared to theoretical value. In the case of tangential compression, the average peak load obtained from the experiment is higher than theoretical value because of the additional bonding strength (confining strength) provided by top and bottom GFRP skins that further strengthen the tangential compressive strength of specimens. Based on experiment and theoretical prediction, the longitudinal compression strength of specimen is stronger than its tangential compression strength. This is attributed to stronger longitudinal compressive property of GFRP skins as compared to its tangential characteristic. In general, the results obtained from theoretical prediction of are reasonably comparable with the failure loads obtained from the experiment. The discrepancies among these values are attributed to the assumptions and idealizations made in failure load estimation.

Table 4. Experimental and theoretical failure loads

Test	Experimental (kN)	Theoretical (kN)
Flexure	53.45	54.74
Shear	211.73	121.20
Longitudinal Compression	450.05	527.00
Tangential Compression	220.31	166.67

CONCLUSIONS

This paper presented an investigation of the physical and mechanical behaviour of hybrid FRP composite beam. Based on the results, the following conclusions are drawn:

- (1) Failures of beam in flexure, shear, longitudinal and tangential compression are governed by delamination and buckling of top GFRP skin.
- (2) The stiffness of hybrid beam was enhanced due to the addition of top and bottom GFRP plates. Even though the transverse shear strength of top and bottom GFRP skins are exceeded, the skins continued to resist stresses through its tensile strength.
- (3) The bonding (confining) strength provided by top and bottom GFRP skins improved the transverse compression strength of specimens.
- (4) The longitudinal compression failure load of the beam is higher than its transverse compression load because of the contribution of longitudinal compression strength of top and bottom GFRP plates.
- (5) Generally, experimental results are reasonably comparable with the predicted values. The discrepancies are attributed to the assumptions and idealizations made in failure load estimation.

ACKNOWLEDGEMENT

The authors gratefully acknowledge Mr. Ernesto Guades of CEEFC, USQ for the technical assistance he had extended in this research project.

REFERENCES

- American Society for Testing and Materials (2000). "Standard test method for flexural properties of sandwich constructions (C393-00)", *ASTM International*, West Coschocken (PA).
- American Society for Testing and Materials (1996). "Standard test method for edgewise compressive strength of sandwich constructions (C364-94)", *ASTM International*, West Coschocken (PA).
- APA/EWS (1996). "Load and Resistance Factor Design: Manual for Engineered Wood Construction", *APA-The Engineered Wood Association*, Washington.
- Barbero, E.J. (1999). *Introduction to Composite Materials Design*, Taylor and Francis Group, Great Britain.
- Flores-Johnson, E.A. and Li, Q.M. (2012). "Structural behaviour of composite sandwich panels with plain and fibre-reinforced foamed concrete cores and corrugated steel faces", *Composite Structures*, 94, 1555-1563.
- Issa, C.A. and Kmeid, Z. (2005). "Advanced wood engineering: glulam beams", *Construction and Building Materials*, 19 (2), 99-106.
- Kim, J.H., Lee, Y.S., Park, B.J. and Kim, D.H. (1999). "Evaluation of durability and strength of stitched foam-cored sandwich structures", *Composite Structures*, 47, 543-550.
- Manalo, A.C., Aravinthan, T., Karunasena, W., and Islam M.M. (2009). "Flexural Behaviour of Structural Fibre Composite Sandwich beams in Flatwise and Edgewise Positions", *Composite Structures*, 92(4), 984-995.
- Manalo, A.C., Aravinthan, T., and Karunasena, W. (2010). "In-plane Shear Behaviour of Fibre Composite Sandwich Beams using Asymmetrical Beam Shear Test", *Construction and Building Materials*, 24, 1952-1960.
- Manalo, A.C (2011). "Behaviour of Fibre Composite Sandwich Structures: A Case Study on Railway Sleeper Application", *PhD Dissertation FOES, USQ*.
- Zhou, G., Forbes A.J. and Foste, N (1999). "Static behaviour of preconditioned glass-fibre-reinforced composite epoxy sandwich I-beams", *Composites Science and Technology*, 59, 963-973.